Coulombic Effects of Remote Subsites on the Active Site of Ribonuclease A[†]

Barbra M. Fisher, L. Wayne Schultz, and Ronald T. Raines*

Departments of Biochemistry and Chemistry, University of Wisconsin—Madison, Madison, Wisconsin 53706

Received June 9, 1998; Revised Manuscript Received September 14, 1998

ABSTRACT: The active-site cleft of bovine pancreatic ribonuclease A (RNase A) is lined with cationic residues that interact with a bound nucleic acid. Those residues interacting with the phosphoryl groups comprise the P0, P1, and P2 subsites, with the scissile P−$O_{5'}$ bond residing in the P1 subsite. Coulombic interactions between the P0 and P2 subsites and phosphoryl groups of the substrate were characterized previously [Fisher, B. M., Ha, J.-H., and Raines, R. T. (1998) *Biochemistry 37*, 12121−12132]. Here, the interactions between these subsites and the active-site residues His12 and His119 are described in detail. A protein variant in which the cationic residues in these subsites (Lys66 in the P0 subsite and Lys7 and Arg10 in the P2 subsite) were replaced with alanine was crystallized, both free and with bound 3′-uridine monophosphate (3′−UMP). Structures of K7A/R10A/K66A RNase A and the K7A/R10A/K66A RNase A·3′−UMP complex were determined by X-ray diffraction analysis to resolutions of 2.0 and 2.1 Å, respectively. There is little observable change between these structures and that of wild-type RNase A, either free or with bound 3′-cytidine monophosphate. K7A/R10A/K66A RNase A was evaluated for its ability to cleave UpA, a dinucleotide substrate that does not span the P0 or the P2 subsites. In comparison to the wild-type enzyme, the value of k_{cat} was decreased by 5-fold and that of k_{cat}/K_m was decreased 10-fold, suggesting that these remote subsites interact with the active site. These interactions were characterized by determining the pK_a values of His12 and His119 at 0.018 and 0.142 M Na^+, both in wild-type RNase A and the K7A/R10A/K66A variant. The side chains of Lys7, Arg10, and Lys66 depress the pK_a values of these histidine residues, and this depression is sensitive to the salt concentration. In addition, the P0 and P2 subsites influence the interaction of His12 and His119 with each other, as demonstrated by changes in the cooperativity that gives rise to microscopic pK_a values. Finally, the affinity of 3′−UMP for wild-type RNase A and the K7A/R10A/K66A variant at 0.018 and 0.142 M Na^+ was determined by isothermal titration calorimetry. 3′−UMP binds to the variant protein with 5-fold weaker affinity at 0.018 M Na^+ and 3-fold weaker affinity at 0.142 M Na^+ than it binds to wild-type RNase A. Together these data demonstrate that long-range Coulombic interactions are an important feature in catalysis by RNase A.

Enzymes employ a variety of devices to effect catalysis (*1, 2*), with Coulombic forces[1] being one of the most important. The side chains of four (or five, if histidine is included) of the 20 amino acids bear a charge under physiological conditions. Coulombic forces can create environments that increase association rates of a substrate for an enzyme (*3*), contribute to the stabilization of the catalytic transition state (*4*), or affect the ionization of active-site residues (*5*).

Short-range Coulombic interactions, such as those between neighboring residues, have long been known to contribute to enzymatic catalysis. For example, acetoacetate decarboxylase catalyzes the decarboxylation of acetoacetate to yield acetone and carbon dioxide. The reaction proceeds via a Schiff base intermediate with the active-site residue Lys115. To form the Schiff base, N_ζ of Lys115 must be in its unprotonated form (*6*), which is a minor form of a typical lysine residue (pK_a 10.5) near neutral pH. The pK_a value of Lys115 is perturbed by more than four units (to 6.0) (*7, 8*) by its spatial proximity to N_ζ of Lys116 (*9*). Thus, a Coulombic interaction between Lys115 and Lys116 obviates the need for general base catalysis.

Only recently have the effects of distant, or long-range, Coulombic forces been explored. "Long-range" refers to interactions between residues that do not make direct contact due to distance constraints. For example, Jackson and Fersht altered charged residues 13−15 Å from the active site of

[†] This work was supported by Grant GM44783 (NIH). L.W.S. was supported by postdoctoral fellowship CA69750 (NIH). Calorimetry data were collected at the University of Wisconsin—Madison Biophysical Instrumentation Facility, which is supported by the University of Wisconsin—Madison and Grant BIR-9512577 (NSF). NMR spectroscopy was performed at the National Magnetic Resonance Facility at Madison, which is supported by NIH Grant RR02301 from the Biomedical Research Technology Program, National Center for Research Resources; equipment in the facility was purchased with funds from the University of Wisconsin, the NSF Biological Instrumentation Program (DMB-8415048), NSF Academic Research Instrumentation Program (BIR-9214394), NIH Biomedical Research Technology Program (RR02301), NIH Shared Instrumentation Program (RR02781 and RR08438), and the U.S. Department of Agriculture.

* To whom correspondence should be addressed.

[1] We prefer to use the term *Coulombic* rather than *electrostatic* to describe the force between two point charges. We consider "electrostatic" to be a general term that encompasses Coulombic forces, hydrogen bonds, and dipole−dipole interactions. "Coulombic" is thus a more specific term, referring only to interactions that obey Coulomb's law: $F = q_1q_2/(4\pi\epsilon r^2)$.

10.1021/bi981369s CCC: $15.00
Published on Web 00/00/0000 PAGE EST: 15.3

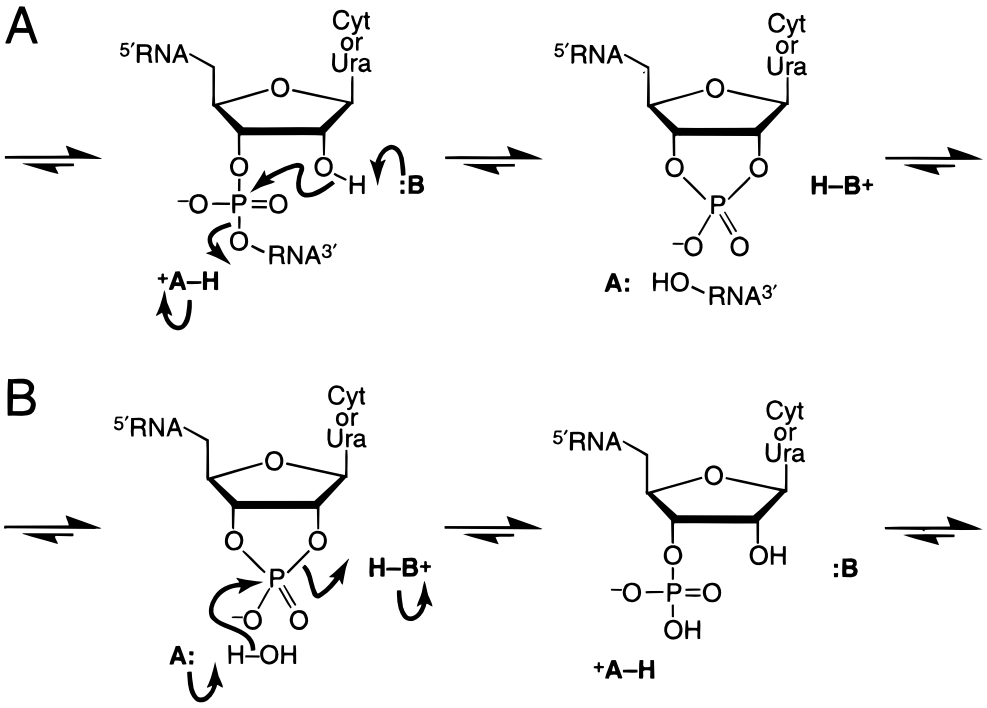

FIGURE 1: Mechanism of the transphosphorylation (A) and hydrolysis (B) reactions catalyzed by ribonuclease A. B is His12, and A is His119 (*11, 12*).

subtilisin BPN′ and found that these alterations affected the binding of a transition-state analogue to the active site (*4*). One of the variants bound to the analogue with 0.6 kcal/mol less free energy than did the wild-type enzyme. These results suggest that long-range Coulombic forces are important for transition-state stabilization. In addition, these results intimate that long-range Coulombic forces could play a significant role in catalysis by other enzymes.

Bovine pancreatic ribonuclease A (RNase A;[2] EC 3.1.27.5), the fourth protein and third enzyme for which a crystal structure had been solved, has been an excellent model system for studying protein structure−function relationships (*10*). RNase A is an endoribonuclease that cleaves and hydrolyzes RNA in two distinct steps (Figure 1). In the first step, the imidazole side chain of His12 acts as a base to abstract a proton from the 2′-hydroxyl of a substrate, thereby facilitating its nucleophilic attack on phosphorus. The imidizolium side chain of His119 acts as an acid to protonate the 5′-oxygen, facilitating its displacement (*11, 12*). Both products are then released to solvent. The slow hydrolysis of the 2′,3′-cyclic phosphodiester occurs in a separate step that resembles the reverse of transphosphorylation (*13, 14*).

His12 and His119 are the acid and base, respectively, in the transphosphorylation reaction catalyzed by RNase A. These assignments were deduced from chemical modification studies, pH-rate profiles (*15, 16*), X-ray diffraction analyses (*17*), and site-directed mutagenesis experiments (*12, 18*−*20*). The pK_a values of these histidine residues have been investigated in detail with ^{1}H NMR spectroscopy (*21*−*28*).

We are interested in the effect of long-range Coulombic forces on the active-site environment of RNase A. In an earlier paper (*29*), we evaluated the role of RNase A residues Lys7, Arg10, and Lys66 in the binding of polymeric substrates. Coulombic interactions between the cationic side chains of these residues and the anionic phosphoryl groups of RNA contribute significantly to catalysis. Here, we have used X-ray diffraction analyses to determine the structure of K7A/R10A/K66A RNase A, both with and without bound uridine 3′-phosphate (3′−UMP). After demonstrating the similarity of these structures to that of wild-type RNase A, with and without bound cytidine 3′-phosphate (3′−CMP), we used steady-state kinetics, ^{1}H NMR spectroscopy, and isothermal titration calorimetry to show that the importance of these residues *extends beyond* their roles in RNA binding. Indeed, Lys7, Arg10, and Lys66 are important not only for creating a cationic environment that attracts polyanionic RNA but also for depressing the pK_a values of active-site residues His12 and His119. Together, these results suggest the importance of long-range Coulombic interactions in the catalysis of RNA cleavage by RNase A.

EXPERIMENTAL PROCEDURES

Materials. Wild-type and K7A/R10A/K66A RNase A were produced in *Escherichia coli* strain BL21(DE3) as described elsewhere (*29*). 2-(*N*-Morpholino)ethanesulfonic acid (MES), obtained as the free acid, was from ICN Biomedicals (Aurora, OH). Uridylyl(3′→5′)adenosine (UpA), synthesized by the methods of Ogilvie (*30*) and Beaucage and Caruthers (*31*), was a generous gift of J. E. Thompson. 3′−UMP was from Sigma (St. Louis, MO). Deuterium oxide (D_2O; 99%) was from Aldrich Chemical (Milwaukee, WI). Deuterium chloride solution (DCl; 35% v/v in D_2O) and sodium deuteroxide solution (NaOD; 40% v/v in D_2O) were

[2] Abbreviations: 3′−CMP, cytidine 3′-phosphate; CpA, cytidylyl(3′→5′)adenosine; C>p, cytidine 2′,3′-cyclic phosphate; DCl, deuterium chloride; D_2O, deuterium oxide; DSS, sodium 2,2-dimethyl-2-silapentane-5-sulfonate; IEF, isoelectric focusing; MES, 2-(*N*-morpholino)-ethanesulfonic acid; NaOD, sodium deuterioxide; PDB, Protein Data Bank, which is maintained by the Brookhaven National Laboratory; pI, isoelectric point; ppm, parts per million; ^{1}H NMR, proton nuclear magnetic resonance; RNase A, bovine pancreatic ribonuclease A; 3′−UMP, uridine 3′-phosphate (otherwise Up); UpA, uridylyl(3′→5′)-adenosine; U>p, uridine 2′,3′-cyclic phosphate.

from Isotech (Miamisburg, OH). Sodium 2,2-dimethyl-2-silapentane-5-sulfonate (DSS) was from Cambridge Isotope Laboratories (Andover, MA). Sigmacote was from Sigma. All other chemicals and reagents were of commercial grade or better and were used without further purification.

General Methods. Ultraviolet and visible absorbance measurements were made with a Cary Model 3 spectrophotometer equipped with a Cary temperature controller from Varian (Sugar Land, TX). RNase A concentrations were determined by assuming that $\epsilon^{0.1\%} = 0.72\ M^{-1}\ cm^{-1}$ at 277.5 nm (*32*). 3′−UMP concentrations were determined by assuming that $\epsilon_{260} = 10\,000\ M^{-1}\ cm^{-1}$ at pH 7.0 (*33*). pH was measured with a Beckman pH meter fitted with a Corning electrode, calibrated at room temperature with standard buffers from Fisher (Chicago, IL). Buffer solutions were prepared from the free acid of MES. The [Na^+] in these solutions was determined using the Henderson−Hasselbalch equation[3] and assuming a pK_a value of 6.15 for MES at 25 °C (*34*).

Structural Analyses. Investigation of protein structures was performed on a Personal Iris 4D/TG workstation from Silicon Graphics (Mountain View, CA) using the program MIDAS (*35*). The Brookhaven Protein Data Bank (PDB) entry 1rph (*36*) was used to determine distances in native RNase A between Lys7, Arg10, or Lys66 and the active-site histidine residues (His12 or His119). This structure was also used to create electrostatic molecular surface maps of RNase A using the program GRASP (*37*). The electrostatic surfaces are based on the charges of RNase A residues at pH 6.0.

Isoelectric Focusing. The isoelectric point (pI) of K7A/R10A/K66A RNase A was determined using a model 111 Mini IEF Cell from Bio-Rad (Hercules, CA) and a polyacrylamide (5% w/v) gel with Pharmolytes ampholytes (3% w/v; pI range 8−10.5) from Pharmacia (Piscataway, NJ). Focusing was carried out in a stepped fashion (100 V for 15 min, 200 V for 15 min, 450 V for 60 min) in a sealed environment flushed continuously with N_2(g). In addition, strips of Whatman paper soaked in NaOH (1 M) were placed on the bottom of the focusing apparatus to scavenge CO_2 and thereby reduce pH drift caused by CO_2 absorption by the ampholytes (*38*). The pI of K7A/R10A/K66A RNase A was determined by comparing its migration to that of the ampholytes. Strips from both sides of the polyacrylamide gel were cut into 0.5 cm pieces and placed in 1.6 mL microcentrifuge tubes filled with 0.5 mL of H_2O to remove the ampholytes. After 20 min of shaking, the tubes were spun to pellet gel solids. The pH of the eluant was checked and a plot of pH vs distance was constructed (*39*). The migration distance of K7A/R10A/K66A RNase A was measured in order to determine its pI. Similarly, the migration distance of a chymotrypsin standard [pI 8.8 (*40*)] was measured to validate this technique for determining pI values.

Crystallization. Protein crystals were prepared by vapor diffusion using the hanging drop method. Lyophilized K7A/R10A/K66A RNase A was dissolved in unbuffered water to a concentration of 60 mg/mL. Drops consisting of protein solution (1.5 μL), water (1.5 μL), and reservoir solution (3.0 μL) were suspended from coverslips coated with Sigmacote (to prevent protein from adhering to the coverslip surface) over 0.5 mL of reservoir solution [0.1 M sodium acetate buffer (pH 4.5) containing 36% (w/v) poly(ethylene glycol) 4000]. Trigonal crystals of K7A/R10A/K66A RNase A appeared within 3 days of incubation at 20 °C and grew to a final size of 0.4 mm × 0.4 mm × 0.5 mm.

Crystals of K7A/R10A/K66A RNase A containing bound 3′−UMP were prepared by soaking native crystals for 2 days at 20 °C in mother liquor to which 3′−UMP was added to a final concentration of 5 mM.

X-ray Diffraction Data Collection. The crystals of K7A/R10A/K66A RNase A were of space group $P3_221$, with $a = 68.15$ Å, $c = 65.51$ Å, $\alpha = \beta = 90°$, and $\gamma = 120°$. Minor changes in cell constants were observed for crystals soaked with 3′−UMP, with $a = 69.62$ Å and $c = 66.98$ Å. All X-ray data were collected with a Siemens HI-STAR detector mounted on a Rigaku rotating anode operating at 50 kV, 90 mA, and a 300 μm focal spot. The X-ray beam was collimated by double focusing mirrors. The crystal-to-detector distance was 12.0 cm. Data were obtained in 512 × 512 pixel format, processed with the program XDS (*41*, *42*), and scaled using the program Xscalibre (G. E. Wesenberg and I. Rayment, unpublished results). Frames of data ($900 \times 0.15° = 135°$) were collected from single crystals using a single ϕ-scan for both K7A/R10A/K66A RNase A and the K7A/R10A/K66A RNase A·3′−UMP complex. Reflections with I/σ of <0.33 were rejected. The crystals were cooled in a 0.5 °C air stream, resulting in negligible crystal decay for the entire data collection. Full crystallographic details are listed in Table 1.

Refinement of the K7A/R10A/K66A RNase A Structure. The starting model consisted of residues 1−124 of D121A RNase A (*43*) that was stripped of all solvent molecules. The model was subjected to 10 cycles of least-squares refinement using TNT (*44*) and gave an initial *R*-factor of 0.217. Positive and negative $F_o - F_c$ showed clearly that residues 7, 10, and 66 had indeed been replaced with alanine. Manual adjustments to the model were performed in FRODO (*45*). After several cycles of manual adjustments and least-squares refinement, water molecules were added to the model. The peak searching algorithm in TNT was used to place ordered water molecules. Water molecules were retained if they had at least 1σ of $2F_o - F_c$ density, 3σ of $F_o - F_c$ density, and were within hydrogen-bonding distance of the protein or other water molecules.

Refinement of the Structure of the K7A/R10A/K66A RNase A·3′−UMP Complex. The starting model consisted of residues 1−124 of K7A/R10A/K66A RNase A that was stripped of all solvent molecules. The model was subjected to 10 cycles of least-squares refinement using TNT (*44*) and gave an initial *R*-factor of 0.232. A positive $F_o - F_c$ map contoured at 3σ showed clearly the position of 3′−UMP in the active site. Non-active-site water molecules were added at this point using the crystalline structure of K7A/R10A/K66A RNase A as a guide, and the model was subjected to cycles of manual adjustment and least-squares refinement. Then, the 3′−UMP was built into the $F_o - F_c$ density and refined using geometric restraints provided by TNT. The solvent-accessible surface area buried upon K7A/R10A/K66A RNase A binding to 3′−UMP was determined using the program GRASP (*37*). A 1.4 Å spherical probe, which mimics a water molecule, was rolled over the van der Waals surface of K7A/R10A/K66A RNase A and 3′−UMP and of

[3] Using the Henderson−Hasselbalch equation, 0.10 M MES-NaOH buffer (pH 6.0) has a [Na^+] of 0.042 M.

Table 1: X-ray Diffraction Analysis Statistics

crystal data	K7A/R10A/K66A RNase A	K7A/R10A/K66A RNase A·3′−UMP
space group	$P3_221$	$P3_221$
cell dimensions (Å)		
a	68.15 ± 0.01	69.62 ± 0.01
b	68.15 ± 0.01	69.62 ± 0.01
c	65.51 ± 0.02	66.98 ± 0.02
protein molecules/unit cell	6	6
crystallization conditions	PEG 4000 (36% w/v), sodium acetate buffer (pH 4.5)	PEG 4000 (36% w/v), sodium acetate buffer (pH 4.5)
	Data Collection Statistics	
resolution (Å)	2.0	2.1
no. of measured reflections	33 804	33 552
no. of unique reflections	14 929	14 210
avg redundancy	2.3	2.4
avg I/σ	20.1	19.8
completeness (30−2.0 Å) (%)	91	88
completeness high-resolution shell (%)	(2.1−2.0 Å) 84	(2.2−2.1 Å) 88
R_{sym}[a]	0.029	0.026
R_{sym} high-resolution shell	(2.1−2.0 Å) 0.171	(2.2−2.1 Å) 0.122
	Final Refinement Statistics	
RNase A atoms	937	941
3′−UMP atoms		21
solvent atoms	84	94
R-factor[b]	(30−2.0 Å) 0.174	(30−2.1 Å) 0.168
RMS deviation from ideal geometry		
bond distances (Å)	0.010	0.011
bond angles (deg)	2.2	2.2
average *B*-factors (Å^2)		
main-chain atoms	37.8	36.7
side-chain + solvent atoms	42.6	40.5
3′−UMP		40.0

[a] $R_{sym} = \sum_{hkl}|I - \langle I\rangle|/\sum_{hkl}I$, where I is the observed intensity and $\langle I\rangle$ is the average intensity obtained from multiple observations of symmetry related reflections. [b] $R = \sum_{hkl}|F_o - F_c|/\sum_{hkl}|F_o|$, where F_o and F_c are the observed and calculated structure factors, respectively.

the K7A/R10A/K66A RNase A·3′−UMP. The solvent-accessible surface area buried during complex formation was calculated from these values.

Comparison of Variant Structures to that of Wild-Type RNase A. The K7A/R10A/K66A RNase A structure is compared here to that of wild-type RNase A that was likewise crystallized from high salt in the $P3_221$ space group [PDB entry 1rph (*36*)]. This wild-type RNase A structure was solved to a resolution of 2.2 Å. The structure of the K7A/R10A/K66A RNase A·3′−UMP complex is compared here to that of the wild-type RNase A·3′−CMP structure of the same space group that was prepared by soaking native crystals in a solution of 3′−CMP [PDB entry 1rpf (*36*)]. This structure was solved to a resolution of 2.2 Å. RMS deviations were determined from a least-squares superposition of the two structures being compared with the program MIDAS (*35*).

Steady-State Kinetic Analysis. Spectrophotometric assays were used to determine the steady-state kinetic parameters for the cleavage of UpA. The cleavage of UpA was monitored by following a decrease in absorbance at 286 nm as the products of the reaction, U>p and adenosine, were formed. The $\Delta\epsilon$ for this reaction is -620 M^{-1} cm^{-1} at 286 nm (*46*). Assays were performed at 25 °C in 0.10 M MES-NaOH buffer (pH 6.0) containing NaCl (0.10 M). The values of k_{cat}, K_m, and k_{cat}/K_m were determined from initial velocity data with the program HYPERO (*47*).

NMR Spectroscopy. ^{1}H NMR spectroscopy was used to determine the pK_a values of three of the four histidine residues in wild-type RNase A and K7A/R10A/K66A RNase A at two [Na$^+$]. Prior to performing pH titrations of these proteins, exchangeable hydrogens were replaced with deuterium. To exchange deuterium for hydrogen, protein (20 mg) that had been dialyzed exhaustively against water and lyophilized was dissolved in D_2O (1 mL), lyophilized, dissolved again in D_2O (1 mL), and lyophilized again. The pH*, which was a direct pH reading and not corrected for the deuterium isotope effect, was adjusted to 3.0 with DCl and the solution was heated to 60 °C for 1 h to exchange amide protons (*25*). Half of this solution was then removed and adjusted to pH* 9.0 with NaOD. To remove salt introduced during sample preparation, the solution was diluted 10-fold by the addition of D_2O and concentrated by centrifugation filtration using a Centriprep-10 from Amicon (Beverly, MA) that had been prerinsed with D_2O. Two additional 5-fold dilutions and concentrations by centrifugation filtration were performed, effectively reducing the salt concentration by approximately 250-fold. The final concentration step was repeated until the sample volume was <0.5 mL. The solution analyzed by ^{1}H NMR spectroscopy contained protein (0.56 mM), NaCl (0.018 or 0.142 mM), and DSS (0.5 mM). During the experiment, pH* was adjusted using the protein solutions. The pH* 9 protein solution was added to the low pH* solution to raise the pH* and the pH* 3 solution was added to the high pH* solution to lower the pH*, until the two solutions approached the midpoint of the titration, pH* 6.0. Using this technique, it was possible to perform each titration at a constant salt concentration and protein concentration.

Proton NMR spectra were acquired in 1D mode on a Bruker DMX 500 MHz NMR spectrometer at 25 °C using 16K data points and an acquisition time of 1.5 s, with 64, 128, or 256 scans following four dummy scans. Chemical shifts of the histidine C-2 protons, based on the assignments

of Markley (*25*), are reported relative to DSS. Data were fitted using the program MATHEMATICA 3.0 (Wolfram Research; Champaign, IL). Data for His105 were fitted to eq 1, which describes the pH titration of a group with one pK_a. Data for His119, which has two microscopic pK_as, were fitted to eq 2. Data for His12, which has an acidic inflection in the pH* titration in addition to two microscopic pK_as, were fitted to eq 3. Data for His12 and His119 were fitted simultaneously because the difference in the microscopic pK_as for each residue must be identical.

$$\delta_{obs} = \delta_A\delta_{AH^+}\left(\frac{1+\frac{K_{105}}{[H^+]}}{\delta_A+\delta_{AH^+}\frac{K_{105}}{[H^+]}}\right) \quad (1)$$

$$\delta_{obs} = \delta_A\delta_{AH^+}\left(\frac{1+\frac{K_{12a}K_{119b}+K_{119a}[H^+]}{[H^+](K_{12a}+[H^+])}}{\delta_A+\delta_{AH^+}\frac{K_{12a}K_{119b}+K_{119a}[H^+]}{[H^+](K_{12a}+[H^+])}}\right) \quad (2)$$

$$\delta_{obs} = \delta_A\delta_{AH^+}\left(\frac{1+\frac{K_{12a}K_{119b}+K_{12a}[H^+]}{[H^+](K_{119a}+[H^+])}}{\delta_A+\delta_{AH^+}\frac{K_{12a}K_{119b}+K_{12a}[H^+]}{[H^+](K_{119a}+[H^+])}}\right) - \delta_o\left(\frac{\delta_o-\delta_{oH^+}}{\delta_o+\delta_{oH^+}\frac{K_o}{[H^+]}}\right) \quad (3)$$

In eq 2 and 3, the "a" subscript refers to the microscopic pK_a of one active-site histidine residue when the other active-site histidine residue is protonated and the "b" subscript refers to the microscopic pK_a of this histidine when the other histidine residue is unprotonated. In eq 3, K_o refers to the pK_a of the acidic inflection in the His12 titration curve. Equations 1−3 are analogous to those used by Schechter and co-workers (*48*) and us (*49*).

Isothermal Titration Calorimetry. The binding affinities of 3′−UMP for wild-type and K7A/R10A/K66A RNase A were determined by using a Micro Calorimetry System isothermal titration calorimeter from MicroCal (Northampton, MA). All buffer and protein samples were degassed by vacuum prior to use. For the experiment at 0.142 M Na^+, RNase A was in the reaction cell at an initial concentration of 0.4 mM. For the experiment at 0.018 M Na^+, RNase A was in the reaction cell at an initial concentration of 0.12 mM. Following thermal equilibration of the system, there was a delay of 600 s before the first injection. Successive injections (48) of 3′−UMP (5 μL of a 9.2 mM or 3.0 mM solution) were made into the cell at 240 s intervals, and heats of binding were measured after each injection. Binding at the higher [Na^+] was measured at 25 °C in 0.10 M MES-NaOH buffer (pH 6.0) containing NaCl (0.10 M final [Na^+]). The lower salt concentration experiments were performed in 0.020 M MES-NaOH buffer (pH 6.0) containing NaCl (0.010 M final [Na^+]). The reference cell, acting only as a thermal reference to the sample cell, was filled with water.

The least-squared estimates of binding parameters n, $\Delta H°$, and K_d were determined from the raw data using the program ORIGIN (MicroCal Software; Northampton, MA). Values of $\Delta G°$ and $T\Delta S°$ were determined from values of $\Delta H°$ and K_d by using eq 4.

$$\Delta G° = RT \ln K_d = \Delta H° - T\Delta S° \quad (4)$$

The first data point in the sequence was omitted during data processing due to error in the accurate delivery of a particular volume of sample during the first injection.

RESULTS

Isoelectric Point of K7A/R10A/K66A RNase A. The pI of K7A/R10A/K66A RNase A was determined by isoelectric focusing to be 8.3 (data not shown). As expected for a protein variant with several cationic residues replaced with neutral residues, this value is lower than that for the wild-type protein, which has pI 9.3 (*40*). In addition to determining this value, the presence of a single band in the lane corresponding to K7A/R10A/K66A RNase A testifies to its purity.

Crystalline Structures. The statistics for X-ray diffraction analyses of K7A/R10A/K66A RNase A (with and without bound 3′−UMP) are listed in Table 1. The final model for K7A/R10A/K66A RNase A contains the complete protein (residues 1−124), 84 water molecules, and an acetate ion. The *R*-factor for all data in the range 30−2.0 Å is 0.174. The RMS deviations for target geometries are 0.010 Å for bond lengths and 2.2° for bond angles. Average *B*-factors for the main chain and side chains are 37.8 and 42.6 Å^2, respectively. Atomic coordinates for K7A/R10A/K66A RNase A have been deposited in the PDB with accession code 3rsk.

The final model for the K7A/R10A/K66A RNase A·3′−UMP complex contains the complete protein (residues 1−124), 3′−UMP, and 94 water molecules. The *R*-factor for all data in the range 30−2.1 Å is 0.168. The RMS deviations for target geometries are 0.011 Å for bond lengths and 2.2° for bond angles. Average *B*-factors for the main chain, side chains, and 3′−UMP are 36.7, 40.5, and 40.0 Å^2, respectively. Atomic coordinates for the K7A/R10A/K66A RNase A·3′−UMP complex have been deposited in the PDB with accession code 4rsk.

The structures of residues 2−10 and the active site of K7A/R10A/K66A RNase A, superimposed on the wild-type RNase A structure [PDB entry 1rph (*36*)], are shown in Figure 2, panels A and B. Shown in Figure 2C is the structure of the active site of K7A/R10A/K66A RNase A with bound 3′−UMP, superimposed on the same region of the wild-type RNase A·3′−CMP complex [PDB entry 1rpf (*36*)].

Steady-State Kinetic Parameters. Replacing Lys7, Arg10, and Lys66 with alanine has an effect on the values of k_{cat}, K_m, and k_{cat}/K_m for cleavage of UpA (Table 2). The k_{cat} for UpA cleavage by K7A/R10A/K66A RNase A is 5-fold less than that of the wild-type enzyme and the K_m is increased by 2-fold. Accordingly, the k_{cat}/K_m is reduced 10-fold relative to that of wild-type RNase A.

Histidine pK_a Values. The pK_a values for His12, His119, and His105 of RNase A can be determined by analyzing the shift of the imidazolyl C-2 proton upon changing pH* (*25*). The other histidine residue in RNase A, His48, is inaccessible to solvent and its titration curve shows anomalous behavior

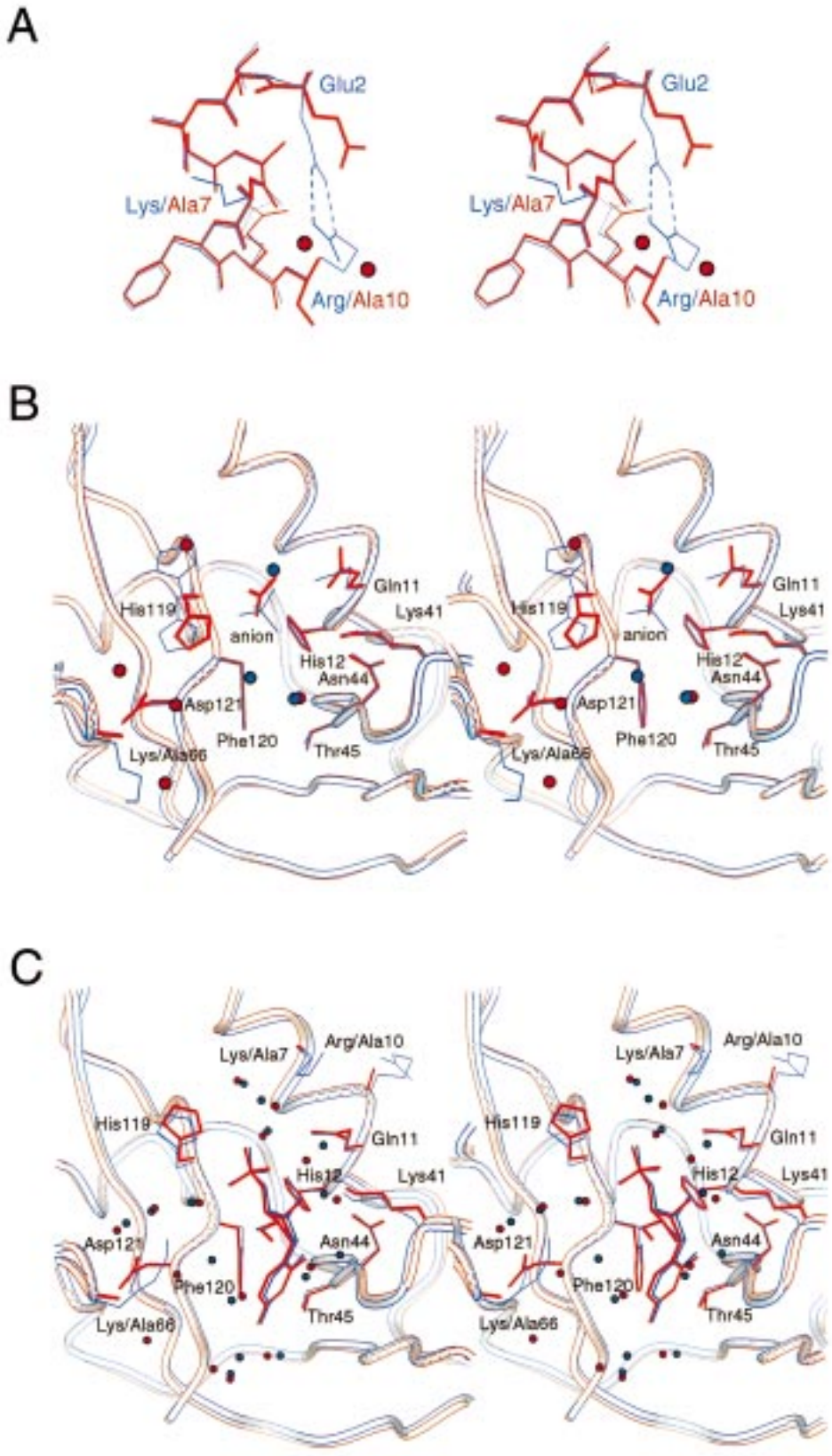

FIGURE 2: Stereoviews of the least-squares superpositions of crystalline ribonucleases. Water molecules are depicted for the variant (red spheres) and wild-type (purple spheres) proteins. This figure was created with the program MOLSCRIPT (*73*). (A) Residues 2−10 of K7A/R10A/K66A ribonuclease A and wild-type ribonuclease A [PDB entry 1rph (*36*)]. Residues of the variant protein (thick red lines) are overlayed on those of the wild-type protein (thin purple lines). Salt bridges between Glu2 and Arg10 of the wild-type protein are indicated by dashed lines. (B) Active sites of K7A/R10A/K66A ribonuclease A and wild-type ribonuclease A [PDB entry 1rph (*36*)]. The variant protein (thick red lines) has an acetate ion in its active site. The wild-type protein (thin purple lines) has a sulfate ion in its active site. (C) Active sites of the K7A/R10A/K66A ribonuclease A·3′−UMP complex (thick red lines) and the wild-type ribonuclease A·3′−CMP complex [(thin purple lines); PDB entry 1rpf (*36*)].

Table 2: Steady-State Kinetic Parameters for the Cleavage of UpA by Wild-Type Ribonuclease A and K7A/R10A/K66A Ribonuclease A[a]

RNase A	k_{cat} (s^{-1})	K_m (mM)	k_{cat}/K_m (10^6 M^{-1} s^{-1})
wild-type	347 ± 40	0.20 ± 0.06	1.7 ± 0.3
K7A/R10A/K66A	70 ± 9	0.39 ± 0.10	0.18 ± 0.03

[a] Data were obtained at 25 °C in 0.10 M MES-NaOH buffer (pH 6.0) containing NaCl (0.10 M).

with pH*, preventing a determination of its pK_a value (*27*). Shown in Figure 3 is the pH* titration of wild-type and K7A/R10A/K66A RNase A at 0.142 and 0.018 M Na^+. His105 is solvent exposed and its titration curve can be fitted to a model with a single pK_a. In contrast, His12 and His119 interact with each other, necessitating the use of a model that includes microscopic pK_as. These microscopic pK_as account for the effect of the protonation state of one histidine residue on the protonation state of the other histidine residue (*28*). In addition, His12 shows an inflection in the acidic region of its pH* titration, necessitating the use of a third pK_a to fit the data accurately. This inflection is due to the titration of a nearby carboxyl group, which perturbs the chemical shift of the C-2 proton of His12 (*50*). This third pK_a value is the least precise of the pK_a values determined due to the lack of data below pH* 3.

The pK_a values of His12, His119, and His105 and the chemical shifts of the protonated and unprotonated forms of these histidine residues in wild-type and K7A/R10A/K66A RNase A at 0.142 and 0.018 M Na^+ are listed in Table 3-(*51*). The pK_a values of His105 in all four pH* titrations are similar, whereas the pK_a values of His12 and His119 differ dramatically in the four pH* titrations. For the wild-type protein, reducing the [Na^+] results in a large decrease in the pK_a values of both His12 and His119. The pK_a values of His12 are decreased by 0.4 units (pK_{12a}) and 0.6 units (pK_{12b}) upon reducing the [Na^+], and the pK_a values for His119 are decreased by 0.5 units (pK_{119a}) and 0.5 units (pK_{119b}) upon reducing the [Na^+]. The pK_a values for K7A/R10A/K66A RNase A are also decreased upon reducing the [Na^+], but to a lesser extent. The pK_a values for His12 are decreased by 0.5 units (pK_{12a}) and 0.4 units (pK_{12b}), and the pK_a values for His119 are decreased by 0.3 units (pK_{119a}) and 0.2 units (pK_{119b}) upon reducing the [Na^+].

A comparison of the His12 and His119 pK_a values in the wild-type and K7A/R10A/K66A proteins, at either salt concentration examined, shows that the cationic side chains of residues 7, 10, and 66 contribute to a depression in these values. When these side chains are removed, the pK_a values of His12 and His119 are increased. These increases are more dramatic at the lower [Na^+] examined than at the higher [Na^+] examined. At 0.018 M Na^+, the pK_a values of His12 are increased by 0.3 units (pK_{12a}) and 0.7 units (pK_{12b}), and the pK_a values of His119 are increased by 0.4 units (pK_{119a}) and 0.8 units (pK_{119b}) upon removing the side chains of residues 7, 10, and 66. At 0.142 M Na^+, the pK_a values of His12 are increased 0.3 units (pK_{12a}) and 0.6 units (pK_{12b}), and the pK_a values of His119 are increased 0.2_5 units (pK_{119a}) and 0.6 units (pK_{119b}) upon removing the side chains of residues 7, 10, and 66.

Binding to 3′−UMP. Shown in Figure 4 are representative data for the calorimetric titrations of wild-type RNase A and the K7A/R10A/K66A variant with 3′−UMP. The thermodynamic parameters derived for these experiments, which were performed at 0.018 and 0.142 M Na^+, are reported in

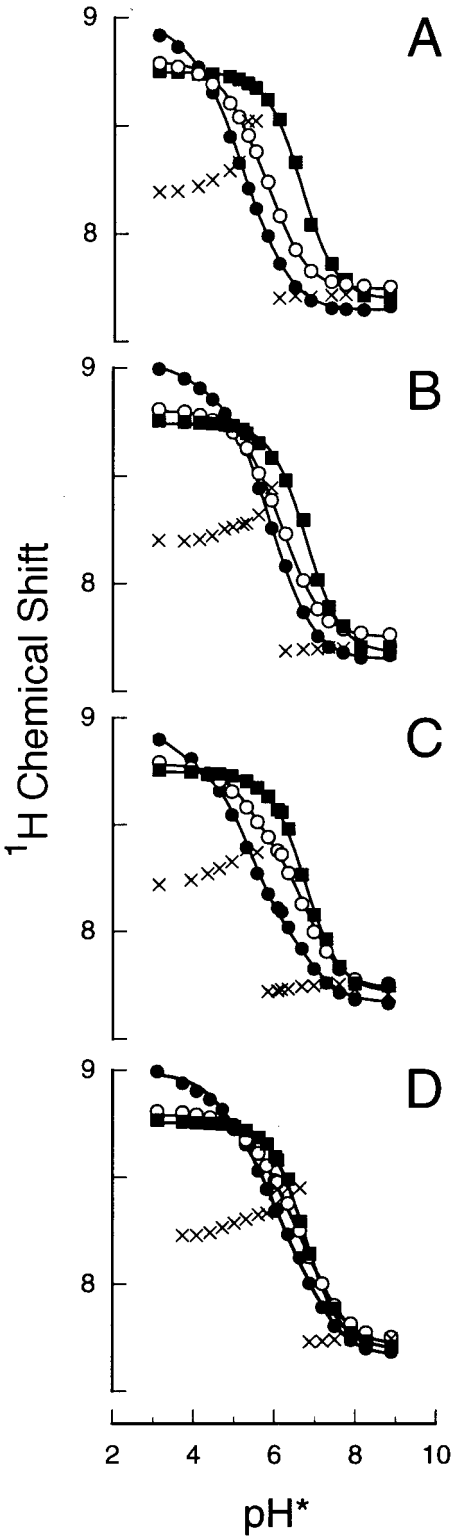

FIGURE 3: pH dependence of the histidine $^1H^{\epsilon 1}$ signals of wild-type ribonuclease A and K7A/R10A/K66A ribonuclease A in D_2O. (A) Wild-type ribonuclease A at 0.018 M Na^+. (B) Wild-type ribonuclease A at 0.142 M Na^+. (C) K7A/R10A/K66A ribonuclease A at 0.018 M Na^+. (D) K7A/R10A/K66A ribonuclease A at 0.142 M Na^+. Chemical shifts are shown for all four histidine residues: His12 (○), His119 (●), His105 (■), and His48 (×). Titrations were carried out at 25 °C. The pK_a values determined from fitting the data to eq 1−3 are listed in Table 3.

Table 3: Microscopic pK_a Values and Chemical Shifts from the Analysis of the pH Dependence of the Chemical Shifts of the $^1H_{\epsilon 1}$ Nuclei of His12, His119, and His105 in Wild-Type Ribonuclease A and K7A/R10A/K66A Ribonuclease A[a]

		wild-type RNase A		K7A/R10A/K66A RNase A	
residue		0.018 M	0.142 M	0.018 M	0.142 M
His12[b]	pK_o	4 ± 1	4.0 ± 0.8	4 ± 1	4.3 ± 0.4
	pK_{12a}	5.3 ± 0.3	5.87 ± 0.05	5.6 ± 0.1	6.15 ± 0.07
	pK_{12b}	5.67 ± 0.09	6.18 ± 0.04	6.4 ± 0.1	6.78 ± 0.08
	δ_{oH+}[c]	9.1 ± 0.3	9.01 ± 0.06	9.1 ± 0.2	9.07 ± 0.05
	δ_{AH+}	8.8 ± 0.3	8.87 ± 0.04	8.8 ± 0.1	8.77 ± 0.06
	δ_A	7.65 ± 0.01	7.65 ± 0.01	7.67 ± 0.03	7.67 ± 0.03
His119[b]	pK_{119a}	5.5 ± 0.2	6.03 ± 0.05	5.9 ± 0.1	6.28 ± 0.04
	pK_{119b}	5.92 ± 0.06	6.34 ± 0.04	6.71 ± 0.07	6.91 ± 0.06
	δ_{AH+}	8.80 ± 0.02	8.80 ± 0.02	8.78 ± 0.03	8.78 ± 0.01
	δ_A	7.74 ± 0.02	7.75 ± 0.02	7.73 ± 0.03	7.72 ± 0.02
His105	pK_{105}	6.70 ± 0.02	6.82 ± 0.03	6.80 ± 0.02	6.81 ± 0.01
	δ_{AH+}	8.74 ± 0.01	8.74 ± 0.01	8.75 ± 0.01	8.75 ± 0.00
	δ_A	7.69 ± 0.01	7.68 ± 0.01	7.72 ± 0.01	7.70 ± 0.01

[a] Data were obtained at 25 °C with a Bruker DMX 500 MHz NMR spectrometer. Solutions contained protein (0.56 mM), NaCl (0.018 or 0.142 M), and DSS (0.5 mM). Values were determined by fitting the experimental data to eq 1 for His105, eq 2 for His119, and eq 3 for His12. Errors were determined by a nonlinear least-squares fit of the data to eq 1−3. Chemical shift values are in parts per million. [b] Microscopic pK_a values are reported for His12 and His119. [c] The value for δ_o was defined to be 8.86 (*51*).

Table 4. These conditions are similar to those used in our NMR experiments. Replacing Lys7, Arg10, and Lys66, which are all remote to the enzymic active site, with alanine residues results in a decrease in binding affinity for 3′−UMP at both [Na^+] concentrations examined. The affinity of both proteins for 3′−UMP is greater under the lower [Na^+] condition than under the higher [Na^+] condition. The value of K_d for 3′−UMP binding to wild-type RNase A is 9.7 μM at 0.018 M Na^+. The value of K_d increases by 5-fold to 53.8 μM at 0.142 M Na^+. The value of K_d for binding to the K7A/R10A/K66A variant is 47.4 μM at 0.018 M Na^+ and increases by 3-fold to 153.6 μM at 0.142 M Na^+. The binding stoichiometries, *n*, are nearly 1.0 for all four binding experiments, suggesting that a single 3′−UMP ligand binds to each protein molecule under our conditions.

Thermodynamic quantities obtained via calorimetry are apparent quantities. A particular concern is that a measured value of $\Delta H°$ contains a contribution from the protonation/deprotonation of the buffer. This contribution does not alter the value of K_d, but does affect the value of $T\Delta S°$. Hence, the values of $\Delta H°$ and $T\Delta S°$ are not readily interpretable, except perhaps for comparative purposes.

The enthalpies for binding vary slightly, with the enthalpies for binding to the wild-type protein being more exothermic than those for binding to the variant protein. These $\Delta H°$ values are −13.8 and −11.8 kcal/mol for binding to the wild-type protein at the lower and higher [Na^+] conditions, respectively. The $\Delta H°$ values are −10.1 and −9.4 kcal/mol for binding to the K7A/R10A/K66A variant at the lower and higher [Na^+] conditions, respectively. The entropies for binding of 3′−UMP to RNase A appear to depend more on the protein than on the solution condition. The $T\Delta S°$ values for binding to the wild-type protein are −6.8 and −5.8 kcal/mol at the lower and higher [Na^+], respectively. The $T\Delta S°$ value for binding to the variant protein is −4.1 kcal/mol at both solution conditions examined.

DISCUSSION

RNase A is a cationic protein under physiological conditions [pI 9.3 (*40*)]. Its active-site cleft is lined with basic amino acid residues that interact with the RNA substrate during catalysis. The interactions of several of these basic residues with the RNA substrate had been characterized previously. For example, the residues known to interact with the phosphoryl groups on RNA have been shown to belong to one of three phosphoryl group binding pockets, named the P0, P1, and P2 subsites (Figure 5). The active-site residues His12, His119, and Lys41 comprise the P1 subsite. Lys66 comprises the P0 subsite, and Lys7 and Arg10 comprise the P2 subsite. Chemical modification and mutagenesis experiments have been used to characterize these binding pockets (*10*, *52*). In addition, the salt concentration dependence of binding of a single-stranded DNA oligomer to wild-type RNase A and the K66A, K7A/R10A, and K7A/R10A/K66A variants demonstrated that significant Coulombic interactions exist between the side chains of Lys7, Arg10, and Lys66 and the phosphoryl groups of the bound nucleic acid (*29*).

Enzymic residues can be involved in substrate binding and substrate turnover. Distinguishing between these two functions can be problematic. Although the P0 and P2 subsites of RNase A have been characterized extensively in terms of their involvement in substrate binding, their roles in substrate turnover have been described only briefly. Cuchillo and coworkers noted an effect on both K_m and k_{cat} for cleavage of CpA and poly(C), and hydrolysis of C>p when Lys7 and Arg10 were replaced with glutamine residues (*53*). The reductions in k_{cat} upon removing the positive charges in the P2 subsite were not expected, especially for CpA and C>p, which do not interact directly with this subsite. Our results for the cleavage of UpA and poly(C) by variants at positions 7, 10, and 66 are in accord with those of Cuchillo and coworkers. As listed in Table 2, the catalysis of UpA cleavage is compromised by replacement of these residues with alanine. Molecular dynamics calculations indicated that binding of CpA or the transition-state analogue uridine 2′,3′-cyclic vanadate displaces the side chain of Lys7 (*54*). These calculations led Cuchillo and co-workers to suggest that the role of Lys7 during catalysis is to stabilize the transition state through a network of intervening water molecules (*53*). A role for Arg10 and Lys66 during catalysis had not been described previously.

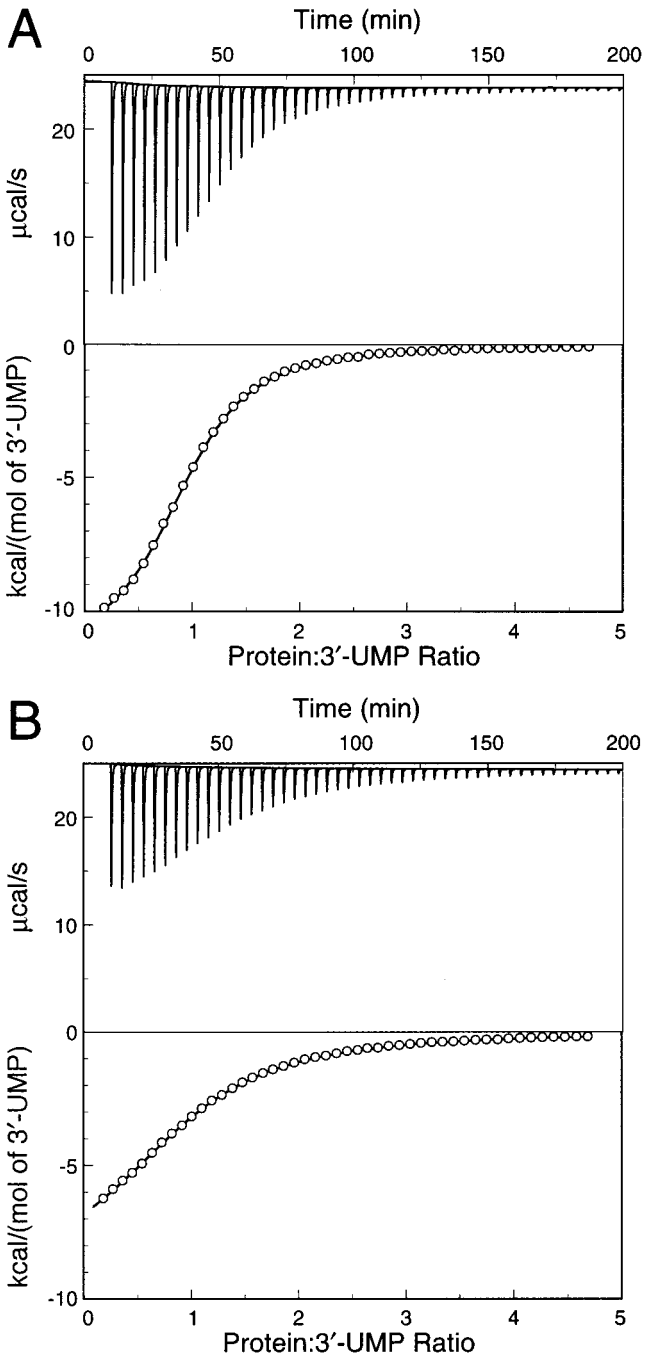

FIGURE 4: Thermograms for the binding of 3′−UMP to wild-type ribonuclease A (A) and K7A/R10A/K66A ribonuclease A (B) at 0.142 M Na^+. The upper graphs show the heat released by the protein solutions upon injection of 3′−UMP. The lower graphs show the heat released upon binding versus the molar ratio of 3′−UMP to ribonuclease. Binding was measured by isothermal titration calorimetry at 25 °C in 0.10 M MES-NaOH buffer (pH 6.0) containing NaCl (0.10 M).

The results of our ^{1}H NMR spectroscopy and calorimetry experiments suggest two roles for Lys7, Arg10, and Lys66. First, the side chains of Lys7, Arg10, and Lys66 enhance the charge of the cationic-binding cleft that attracts the anionic RNA substrate to the enzymic active site. Second, the side chains of Lys7, Arg10, and Lys66 depress the pK_a values of the active-site histidine residues. The impaired catalysis of UpA cleavage by RNase A variants with altered P0 and P2 subsites is explained by a failure to fulfill this second role. Before defining the roles of the Lys7, Arg10, and Lys66 side chains in effecting the active-site environment of RNase A, the structure of the K7A/R10A/K66A variant, both with and without bound 3′−UMP, will be described in detail.

Crystalline Structures. RNase A was one of the first enzymes whose structure was determined by X-ray diffraction analysis (*17*). In total, over 70 sets of three-dimensional coordinates (from both X-ray diffraction analysis and ^{1}H NMR spectroscopy) related to RNase A have been deposited in the PDB (*10*), including structures of RNase A with bound oligonucleotides, dinucleotides, and mononucleotides (*55*, *56*). Recently, we reported the first crystalline structures of active-site variants of RNase A [D121A RNase A; PDB entry 3rsd and D121N RNase A; PDB entry 4rsd (*43*)] as well as that of a variant in which a proline residue with a cis peptide bond had been replaced with glycine [P93G RNase A; PDB entry 3rsp (*57*)]. The crystalline structure of K7A/R10A/K66A RNase A reported here is the first for a distal subsite variant. We also report the first crystalline structure of an RNase A variant with a bound ligand, 3′−UMP. These structures show that replacing Lys7, Arg10, and Lys66 with an alanine residue does not affect the overall structure of RNase A, either with or without bound 3′−UMP. In addition, the similarity of the K7A/R10A/K66A RNase A crystalline structures to the three-dimensional structure of the wild-type protein with and without bound 3′−CMP supports our hypothesis that residues Lys7, Arg10, and Lys66 affect the active-site environment of RNase A via long-range Coulombic interactions and not by perturbing the three-dimensional structure of the enzyme.

The structure of the K7A/R10A/K66A variant of RNase A was solved in the trigonal space group $P3_221$ and contains an acetate ion in the active site. The main-chain atoms of K7A/R10A/K66A RNase A have an average RMS deviation of 0.36 Å from those of wild-type RNase A [PDB entry 1rph (*36*)]. The structure of the K7A/R10A/K66A RNase A·3′−UMP complex was also solved in the trigonal space group $P3_221$ and contains a single 3′−UMP ligand bound in the active site. The main-chain atoms of K7A/R10A/K66A RNase A in the K7A/R10A/K66A RNase A·3′−UMP complex have an average RMS deviation of 0.48 Å from those of the wild-type RNase A·3′−CMP complex [PDB entry 1rpf (*36*)].

P0 and P2 Subsites. There is little observable change in the main-chain atoms of residues 7, 10, and 66 upon replacement with alanine. As shown in Figure 2, panels A and B, the K7A/R10A/K66A RNase A structure contains two water molecules in the position occupied by Arg10 in the wild-type protein structure and a single water molecule in the position occupied by Lys66 in that structure. No ordered water molecules in the place of Lys7 are apparent.

Active Site. In the structure of K7A/R10A/K66A RNase A, we find little change in the positions of the main-chain and side-chain atoms of residues residing in the P1 or B1 (pyrimidine binding) subsites (Figure 5). The position of His12 in the K7A/R10A/K66A RNase A structure has not changed from that in the wild-type structure. The side chain of His119 in RNase A has been shown to occupy two distinct positions, denoted as A and B, which are related by a 100° rotation about the $C_\alpha-C_\beta$ bond and a 180° rotation about the $C_\beta-C_\gamma$ bond (*58, 59*). The position of the His119 side chain has been shown to be dependent on the pH and ionic

Table 4: Thermodynamic Parameters for the Binding of 3′−UMP to Wild-Type Ribonuclease A and K7A/R10A/K66A Ribonuclease A[a]

RNase A	[Na^+] (M)	n	K_d (mM)	$\Delta G°$ (kcal/mol)	$\Delta H°$ (kcal/mol)	$T\Delta S°$ (kcal/mol)
wild-type	0.018[b]	0.93	0.0097	−7.0	−13.8	−6.8
wild-type	0.142[c]	0.95	0.054	−6.0	−11.8	−5.8
K7A/R10A/K66A	0.018	1.00	0.047	−6.1	−10.1	−4.1
K7A/R10A/K66A	0.142	0.96	0.15	−5.3	−9.4	−4.1

[a] Data were obtained at 25 °C by isothermal titration calorimetry. Errors on the curve fitting, determined using the program ORIGIN, were <5%. Errors determined from duplicate experiments were closer to 10%. We therefore assume the real error on the n and K_d values to be ≤10% and the real errors on the $\Delta G°$, $\Delta H°$, and $T\Delta S°$ to be ≤5%. [b] Data at 0.018 M Na^+ were obtained in 0.020 M MES-NaOH buffer (pH 6.0) containing NaCl (0.010 M). [c] Data at 0.142 M Na^+ were obtained in 0.10 M MES-NaOH buffer (pH 6.0) containing NaCl (0.10 M).

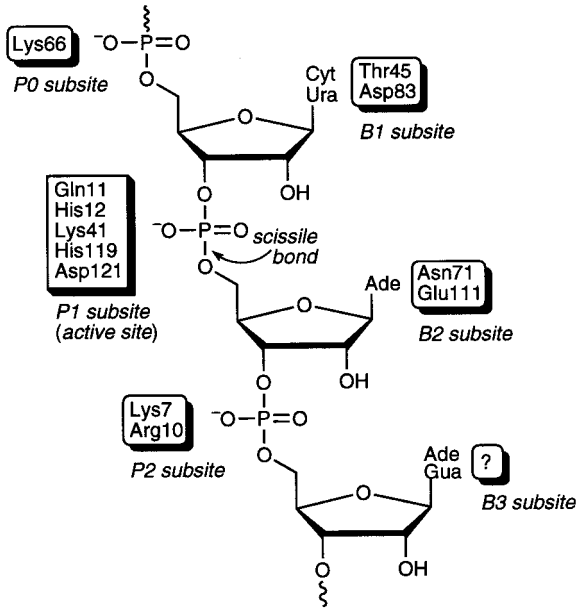

FIGURE 5: Schematic representation of the binding of an RNA fragment to ribonuclease A. The scissile bond is indicated. B and P refer to base and phosphoryl group binding subsites, respectively. In each subsite, the amino acid residues that are known or presumed to be involved in the interaction with RNA are indicated (*10*).

strength of the crystallization solution (*60*). In the wild-type structure used for comparison here, the His119 side chain occupies both positions A and B. In the K7A/R10A/K66A RNase A structure, the side chain of His119 occupies only position A, with a χ_1 angle of 165° (the χ_1 angle in the 1rph structure is also 165°). Although the χ_1 angles for His119 are similar in the variant and wild-type proteins, a superposition of the two structures shows that the His119 side chain position in K7A/R10A/K66A RNase A is altered slightly with respect to His119 in the wild-type structure. This small alteration is presumably due to the presence of an acetate ion, rather than a sulfate ion, bound in the active site. A sulfate ion is considerably larger than an acetate ion [thermochemical radius of 2.58 vs 1.62 Å (*61*)] and occupies a tetrahedral, rather than planar, geometry. In the wild-type structure, the oxygens of the bound sulfate bridge $N_{\epsilon 2}$ of His12 and $N_{\delta 1}$ of His119. Similarly, the oxygens of the bound acetate also bridge $N_{\epsilon 2}$ of His12 and $N_{\delta 1}$ of His119 in the K7A/R10A/K66A RNase A structure. In addition, there is a water molecule in the K7A/R10A/K66A RNase A structure occupying the space taken by the B position of the His119 side chain in the wild-type structure. The positions of the other active-site residues, Gln11, Lys41, and Asp121 in the P1 subsite and Thr45 and the Phe120 main-chain atoms in the B1 subsite, are virtually unchanged between the wild-type and variant crystalline structures.

S-Peptide. In the presence of the protease subtilisin, RNase A is cleaved preferentially between residues 20 and 21 to form S-peptide (residues 1−20) and S-protein (residues 21−124) (*62*). When these two fragments are recombined to form the noncovalent complex RNase S, enzymatic activity is indistinguishable from that of RNase A. Residues 1−15 of S-peptide (S15) are sufficient for binding S-protein and effecting catalysis (*63*). Residues 2−13 of S-peptide form a stable α-helix when bound to S-protein and in isolation, maintains considerable helicity (10−50%) in water (*64*, *65*). This α-helical structure is necessary for stabilizing intermediates in the folding of RNase S (*66*−*68*) and proper alignment of the catalytically important residue His12 in RNase A or RNase S. S-Peptide [and also C-peptide, residues 1−13 of RNase A, terminating in homoserine lactone (*69*)] is frequently used as a model system for studying α-helices; several such studies have focused on the determinants of α-helix formation. A salt bridge between Glu2 and Arg10 plays a fundamental role in the folding of isolated S-peptide (*70*, *71*). Replacement of Glu2 with alanine in C-peptide results in a peptide with no measurable helix formation (*72*).

The structure of the N-terminal residues in K7A/R10A/K66A RNase A is similar to that in the wild-type protein. Lys1 is disordered, but residues 2−15 of the variant protein structure are superimposable on the wild-type protein structure. The average RMS deviation for residues 2−15 of K7A/R10A/K66A RNase A is 0.23 Å from those residues in the wild-type structure. As shown in Figure 2A, K7A/R10A/K66A RNase A has two water molecules in the position occupied by Arg10 in the wild-type structure. Neither of these water molecules are within hydrogen-bonding distance of Glu2 (one water molecule is 4.9 Å away from $O_{\epsilon 1}$ of Glu2 and the other is 5.5 Å away from this atom). Although the $Glu2^-\cdots Arg10^+$ salt bridge is important for α-helix formation in isolated S-peptide, the structure reported herein with alanine at position 10 suggests that this salt bridge is not necessary for α-helix formation in the context of the entire protein.

3′−UMP. The structure of the K7A/R10A/K66A RNase A·3′−UMP complex determined here is similar to that of the wild-type RNase A·3′−CMP complex determined previously (*36*). Still, there are some minor changes between these two complexes due to structural differences between uridine and cytidine. The relevant intermolecular interactions are listed in Table 5. Briefly, 3′−UMP makes contact with the B1 subsite, the P1 subsite, and bound water molecules (Figure 2C), burying 515 $Å^2$ of solvent-accessible surface area of the protein upon binding (*37*). In the B1 subsite, a hydrogen bond mediates the nucleotide specificity of RNase

Table 5: Hydrogen Bonds in the Active Sites of the Wild-Type Ribonuclease A·3′−CMP and K7A/R10A/K66A Ribonuclease A·3′−UMP Complexes

hydrogen bond donor	hydrogen bond acceptor	K7A/R10A/K66A RNase A·3′−UMP[a] (Å)	wild-type RNase A·3′−CMP[b] (Å)
Thr45 $O_{\gamma 1}$	N3	na[c]	2.9
N3	Thr45 $O_{\gamma 1}$	2.8	na
Thr45 N	O2	2.8	2.7
Thr45 $O_{\gamma 1}$	Asp83 $O_{\delta 1}$	3.0	na
Water (206)	O4	2.9	na
His12 $N_{\epsilon 2}$	O2P	3.0	2.7
His12 $N_{\epsilon 2}$	O2′	3.5	2.9
His119 $N_{\delta 1}$	O3P	2.7	3.2
His119 $N_{\delta 1}$	O1P	3.5	3.1
His119 $N_{\epsilon 2}$	water (249)	3.2	na
Lys41 N_{ζ}	O2′	2.7	2.7
Lys41 N_{ζ}	Asn44 $O_{\delta 1}$	3.0	2.7
Lys41 N_{ζ}	Gln11 $O_{\epsilon 1}$	2.9	3.1
Phe120 N	O1P	2.8	2.7

[a] Distances were determined by using the three-dimensional structure reported herein (PDB entry 4rsk) and the program MIDAS (*35*). [b] Data from ref *36*. [c] Not applicable.

A (*74*). In accord with the crystalline complex of RNase A with uridine 2′,3′-cyclic vanadate (*75*), hydrogen bonds are formed between N3 and O2 of bound uridine and $O_{\gamma 1}$ and the main chain N of Thr45, respectively, and between $O_{\gamma 1}$ of Thr45 and $O_{\delta 1}$ of Asp83. In addition, a bound water molecule donates a hydrogen bond to O4 of uridine.

The active-site residues in the K7A/R10A/K66A RNase A·3′−UMP complex are unchanged from those in the wild-type RNase A·3′−CMP complex. The side chains of His12 in the two structures are superimposable, as are those of His119. Both $N_{\epsilon 2}$ of His12 and $N_{\delta 1}$ of His119 donate hydrogen bonds to oxygens of the bound phosphoryl group. In addition, His119 donates a hydrogen bond to a bound water molecule, which is not seen in the wild-type RNase A·3′−CMP crystalline structure. In both the wild-type and variant crystalline structures with bound nucleotide, His119 is in the B position. The χ_1 angle for the His119 side chain in the variant structure is −64°, compared to −69° in the wild-type structure. Further, N_{ζ} of Lys41 donates hydrogen bonds to three atoms: O2′ of the bound nucleotide, $O_{\epsilon 1}$ of Gln11, and $O_{\delta 1}$ of Asn44. The structural similarities between the wild-type and variant free proteins and protein·nucleotide complexes justify our explaining the roles of Lys7, Arg10, and Lys66 in terms of function rather than structure.

pH Titrations—Methodology*. The titration behaviors of His12 and His119 in RNase A are well documented (*76*). The pK_a values of these residues (and His105) in free RNase A and RNase A with a bound nucleotide have been determined in a variety of different solution conditions, including various NaCl concentrations (<0.1−0.4 M) and in the absence and presence of inorganic phosphate. We are interested in the role of Coulombic interactions in RNase A and such interactions are masked by concentrated solutions of electrolytes (*77*). Thus, we performed our experiments both in a solution of much lower salt concentration (0.018 M) than had been reported previously and in a solution of salt concentration (0.142 M) similar to that used in our laboratory for RNase A activity assays (*78*).

The most common method for performing pH titrations involves the addition of acid or base to the sample to change the pH. At high salt concentrations, the change in salt concentration upon adding acid or base is negligible. But at low salt concentrations (such as 0.018 M Na^+), the addition of enough NaOD to change the pH* from 3 to 9 would alter dramatically the salt concentration of the solution. Had we used this method, we would have performed a pH titration *and* an ionic strength titration. Our method, which involves mixing two solutions that differ only in pH*, changes only the pH* of the protein solution during the experiment. His105 serves as a useful control for testing the validity of this method. This residue is solvent exposed and is not known to interact with neighboring residues through Coulombic interactions. Its pK_a value should therefore report on the ability of the acidic and basic protein solutions to meet at the appropriate midpoint of the titration curve. Indeed, the pK_a value of His105 is in gratifying agreement (within 0.12 pK_a units) in wild-type RNase A and the K7A/R10A/K66 variant at both solution conditions examined (Table 3) and is also similar to that reported previously (*26*). This agreement validates our method for varying pH*.

Scheme 1

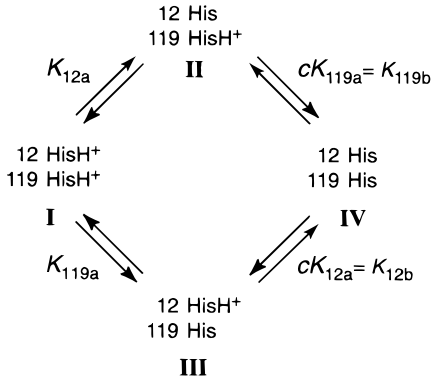

His12 and His119 pK_a Values. If the protonation states of His12 and His119 are influenced by their environment through Coulombic interactions, then their pK_a values should be sensitive to salt concentration. Rüterjans and Witzel have shown that the pK_a values of these residues are influenced by the solution salt concentration and more so than the pK_a values of imidazole or a free histidine residue (*22*). We also find a strong dependence of the His12 and His119 pK_a values on the salt concentration. Unfortunately, a direct comparison of our results to those of Rüterjans and Witzel is not possible because their titrations involved adding base (and hence salt) to their RNase A solutions and their data were not fitted to equations describing microscopic pK_a values.[4]

Microscopic pK_as arise from Coulombic interactions that create either positive or negative cooperativity. In RNase A, the histidine residues interact with positive cooperativity—deprotonation of one histidine residue stabilizes the protonated state of the other histidine residue. As shown in Scheme 1, microscopic pK_a values are related by a thermodynamic box, wherein a complete titration by the path **I** → **II** → **IV** is identical to that by the path **I** → **III** → **IV** (*49*). These four distinct titrations are related by eq 5:

[4] Microscopic pK_a values for His12 and His119 in RNase A were described six years after the publication of the work of Rüterjans and Witzel (*22*).

$$pK_{12a} + p(cK_{119a}) = pK_{119a} + p(cK_{12a}) \quad (5)$$

Equation 5 and the microscopic pK_a values of His12 and His119 (Table 3) can be used to determine the value of $c = K_{12b}/K_{12a} = K_{119b}/K_{119a}$, which provides a measure of the strength of the interaction between His12 and His119. A c value of 1 indicates that no interaction exists between residues and the system need not be described by microscopic pK_a values. In contrast, a c value $\ll 1$ indicates strong negative cooperativity between titratable residues (*79*).

The degree of cooperativity between His12 and His119 in RNase A is affected more by the replacement of Lys7, Arg10, and Lys66 with alanine residues than by the increase in [Na^+]. As listed in Table 6, the deprotonation of His12 and His119 is more cooperative in K7A/R10A/K66A RNase A than in wild-type RNase A. Wild-type RNase A is more cationic than K7A/R10A/K66A RNase A (pI 9.3 vs 8.3; Figure 6, panels B and C). In both proteins, a state in which both histidine residues are protonated is disfavored. But once one histidine is deprotonated, the second histidine is less driven to become deprotonated in the variant protein than in the wild-type protein. This increase in cooperativity upon removal of the three cationic side chains could result from a change in the dielectric constant, ϵ, close to the surface of RNase A. The effect of ϵ on the difference in microscopic pK_a values (ΔpK_a) of an organic acid can be estimated with the Kirkwood−Westheimer equation (*80, 81*):

$$r = \frac{q^2}{2.303\epsilon kT(\Delta pK)} \quad (6)$$

where r is the distance between the two titratable groups (here, His12 and His119), q is the protonic charge, k is Boltzmann's constant, and T is the absolute temperature. Because the distance between His12 and His119 is the same in wild-type RNase A and K7A/R10A/K66A RNase A (Figure 2B) and q, k, and T are constant in both proteins, ΔpK is inversely proportional to the dielectric constant ϵ. Hence, the larger cooperativity (i.e., smaller c value) observed for the deprotonation of His12 and His119 in the variant protein is consistent with a decrease in the effective dielectric constant of the active-site cleft upon removing the cationic side chains of residues 7, 10, and 66.

Why does replacing Lys7, Arg10, and Lys66 with alanine residues have a much larger effect on the cooperativity of the deprotonation of His12 and His119 than does an increase in [Na^+]? The positions of these three point charges, relative to His12 and His119, can be related to that of a single point charge that interacts with the histidine residues in an equivalent manner. We call the distance between this single point charge and the active-site histidine residues the "reduced radius", or "ρ". The value of ρ can be calculated using eq 7 and the distances (r) between n pairs of residues.

$$\rho = \sqrt{\frac{1}{\sum_{i=1}^{n}\left(\frac{1}{r_i}\right)^2}} \quad (7)$$

Equation 7 derives from Coulomb's law, with the concept of reduced radius being analogous to that of reduced mass, μ. The atomic coordinates for the wild-type RNase A crystalline structure [PDB entry 1rph (*36*)] can be used to determine the distances between N_ζ of Lys7, the midpoint of the line segment connecting $N_{\eta 1}$ and $N_{\eta 2}$ of Arg10, and N_ζ of Lys66 and the midpoint of the line segment connecting $N_{\epsilon 2}$ of His12 and $N_{\delta 1}$ of His119. These distances are shown in Figure 7. From eq 7 and these values ($r_1 = 7.6$ Å, $r_2 = 11$ Å, and $r_3 = 14$ Å), we calculate that ρ is equal to 5.7 Å. Thus, this analysis suggests that the three point charges of Lys7, Arg10, and Lys66 are equivalent to a single point charge 5.7 Å from His12 and His119. Interestingly, this value of ρ is only slightly less than is the distance from N_ζ of Lys41 to the midpoint of the line segment connecting $N_{\epsilon 2}$ His12 and $N_{\delta 1}$ His119, which is 6.0 Å (Figure 7). Lys41 is an intimate member of the RNase A active site whose role is to donate a hydrogen bond to the transition state during catalysis (*82*). This residue increases substantially the pK_a values of the active-site histidine residues (J. M. Messmore, B. M. Fisher, and R. T. Raines, unpublished results). Moreover, replacing Lys41 with alanine yields a protein with a c value similar to that of K7A/R10A/K66A RNase A (Table 6).

Table 6: Cooperativity (c) Values from the Analysis of the Microscopic pK_a Values for Wild-Type Ribonuclease A and K7A/R10A/K66A Ribonuclease A[a]

RNase A	[Na^+] 0.018 M	[Na^+] 0.142 M
wild-type	0.40	0.49
K7A/R10A/K66A	0.16	0.23
K41A	0.19[b]	nd[c]

[a] Values of c are average values for His12 and His119 and were calculated with the equation $c = [(K_{12b}/K_{12a}) + (K_{119b}/K_{119a})]/2$ and the data in Table 3. [b] Data from J. M. Messmore, B. M. Fisher, and R. T. Raines (unpublished results). [c] Not determined.

The residue−residue distances can be compared to the residue−sodium ion distances. By using a semiquantitative analysis,[5] we calculate that sodium ions are separated by 45 Å in a 0.018 M Na^+ solution and by 23 Å in a 0.142 M Na^+ solution. These two distances represent averages. Of course, sodium ions are not spaced homogeneously in a solution containing protein; the ionic distribution in the bulk solution differs from that near the protein surface. Nonetheless, the effective molarity of the positive charge from Lys7, Arg10, and Lys66 is much higher than the [Na^+] used in our experiments. Indeed, it would require a solution of 9.0 M NaCl to give an average separation distance of 5.7 Å for each sodium ion. From this analysis, it is not surprising that raising the salt concentration from 0.018 to 0.142 M has little effect on the cooperativity of the deprotonation of His12 and His119 (Table 6).

Implications for Catalysis. General acid−base catalysis is most efficient when the pK_a of the acid−base matches the pH of the solution (*2*). Bases with pK_a values below the solution pH will have a high concentration of unprotonated (i.e., reactive) species, but the reactivity of these species will be low. In contrast, bases with pK_a values above the solution pH will be highly reactive, but the concentration of unprotonated species will be low. A compromise between reactivity and concentration of reactive species is therefore necessary

[5] The average intermolecular distance (r) can be calculated by using Avogadro's number to convert molarity to atom density. Then, $r = (\text{atom density})^{-1/3}$.

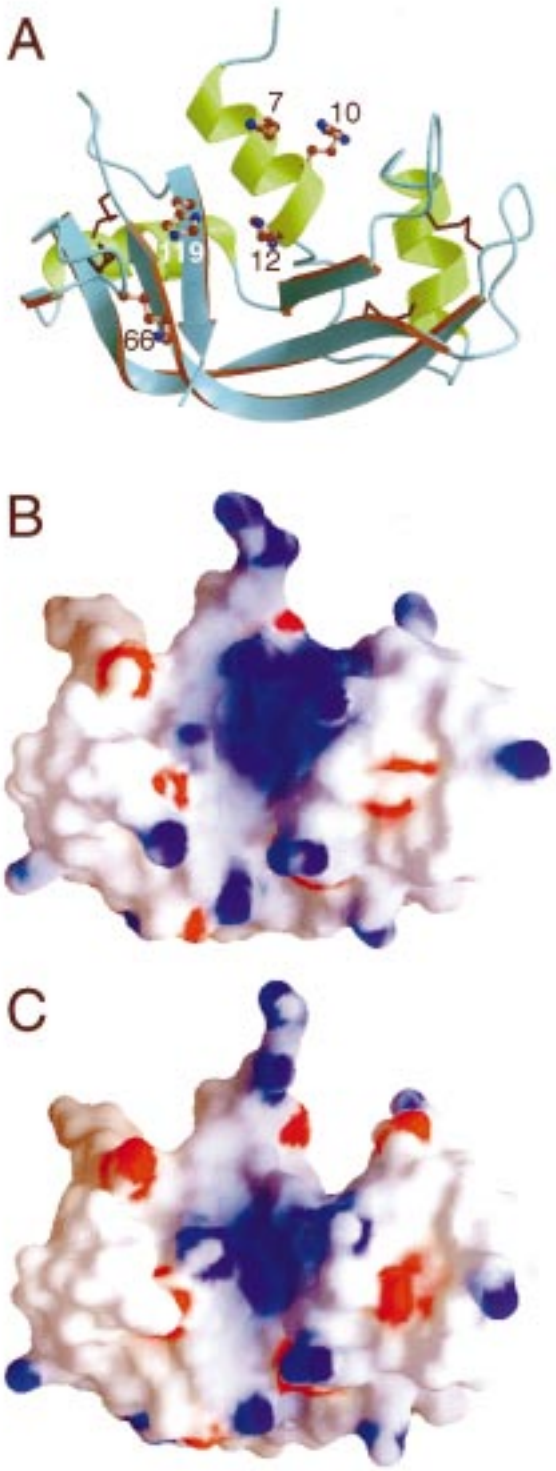

FIGURE 6: Ribbon diagram of wild-type ribonuclease A (A) and electrostatic potential maps of the surface of wild-type ribonuclease A (B) and K7A/R10A/K66A ribonuclease A (C) positioned in the same orientation. Blue denotes regions of positive charge and red denotes regions of negative charge. Charges were calculated for ribonuclease A at pH 6.0 and 0.142 M Na^+ with the pK_a values determined for the active-site histidine residues using ^{1}H NMR spectroscopy (Table 3). The ribbon diagram was created using the program MOLSCRIPT (*73*). Electrostatic potential maps were created with the program GRASP (*37*) and atomic coordinates for wild-type ribonuclease A [PDB entry 1rph (*36*)] and K7A/R10A/K66A ribonuclease A (PDB entry 3rsk).

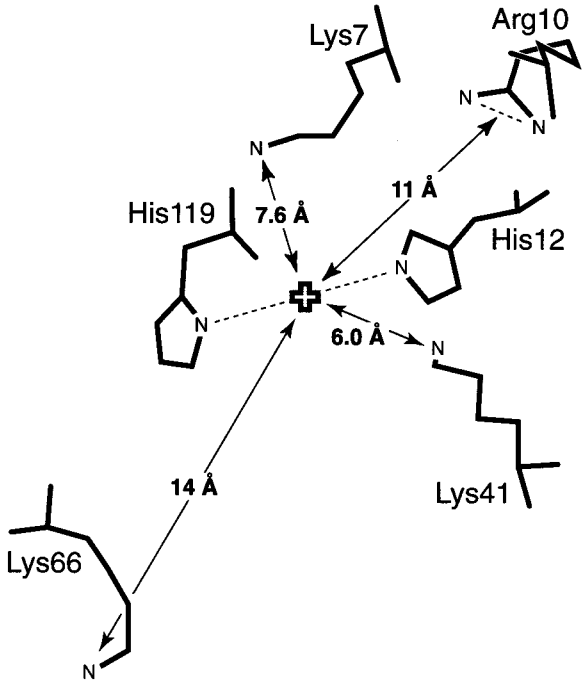

FIGURE 7: Cationic residues near the active site of ribonuclease A. The midpoint of the line segment connecting $N_{\delta 1}$ of His119 and $N_{\epsilon 2}$ of His12 is indicated by a plus sign, and the distances from this point to N_ζ of Lys7, the midpoint of the line segment connecting $N_{\eta 1}$ and $N_{\eta 2}$ of Arg10, N_ζ of Lys66, and N_ζ of Lys41 are shown. Distances were determined by using the atomic coordinates for wild-type ribonuclease A [PDB entry 1rph (*36*)] and the program MIDAS (*35*). The reduced radius of Lys7, Arg10, and Lys66 to the midpoint of the line segment connecting $N_{\delta 1}$ of His119 and $N_{\epsilon 2}$ of His12 was calculated with eq 7 to be $\rho = 5.7$ Å.

for optimal catalytic rates. Indeed, many enzymic active sites contain histidine residues because a typical histidine residue (pK_a 6.4) can act as both an acid and a base at physiological values of pH.

RNase A catalyzes the cleavage and hydrolysis of RNA by general acid−base catalysis, as shown in Figure 1. A pH-rate profile for the cleavage of UpA by wild-type RNase A shows that the pH optimum for this reaction is close to 6.0 (*46*, *83*). The microscopic pK_a values of His12 and His119 in wild-type RNase A are close to this value (Table 3). In contrast, the average of the microscopic pK_a values for His12 and His119 in K7A/R10A/K66A RNase A is 6.5 (at 0.142 M Na^+). Thus, one of the functions of the Lys7, Arg10, and Lys66 side chains is to depress the pK_a values of the active-site histidine residues, and the cleavage of UpA by K7A/R10A/K66A RNase A at pH 6.0 is impaired by a failure to fulfill this role.

RNA polymers are likely to be the natural substrates for RNase A (*13*, *14*). In an earlier paper, we described the role of the Lys7, Arg10, and Lys66 side chains in binding and cleaving polymeric substrates (*29*). Significant Coulombic interactions exist between these cationic side chains and the anionic phosphoryl groups of the substrates. When an RNA strand is bound to RNase A, both the cationic charges in the P0 and P2 subsites and the anionic phosphoryl groups bound in these subsites may form long-range Coulombic interactions with the active-site histidine residues. These repulsive forces and attractive forces should counterbalance, thereby masking the charges on the Lys7, Arg10, and Lys66 side chains with respect to the active-site histidine residues. The result of this effect would be diminished depression of the His12 and

His119 pK_a values when an RNA polymer is bound. The transphosphorylation of dinucleotides and hydrolysis of nucleoside 2′,3′-cyclic phosphates should be affected less by the P0 and P2 subsites than the transphosphorylation of polymeric substrates. Indeed, the optimal pH for the transphosphorylation of UpA and hydrolysis of U>p is close to 6.0 (*46*, *83*) whereas the optimal pH for the transphosphorylation of longer substrates [e.g., $(Up)_4U>p$] is shifted upward by ~1 pH unit (*84*).

Binding to 3′−UMP. Binding of nucleotides to RNase A has been studied as a function of both pH and ionic strength (*85*−*88*). Moreover, the reliability of computer-assisted titration calorimetry for characterizing biochemical binding reactions was first demonstrated with 2′−CMP and RNase A (*89*). It is the dianionic form of 3′−CMP (and presumably 3′−UMP) that binds to RNase A. Although this ligand binds to RNase A when both active-site histidine residues are either protonated or unprotonated, there is a 4.3×10^3-fold preference for complex formation with the doubly protonated form of the enzyme (*90*). At physiological pH, His12 and His119 in RNase A are not protonated fully, prompting a description of complex formation that involves protonation of these residues (*50*, *86*−*88*). This type of binding mechanism, called "proton linkage" because proton binding is linked to ligand binding, is common in protein·ligand complex formation (for examples, see refs *91* and *92*). The increase in the pK_a values of His12 and His119 upon binding 3′−UMP or 3′−CMP (*21*, *24*) is consistent with a proton linkage mechanism for RNase A·nucleotide complex formation.

The positive charges of the Lys7, Arg10, and Lys66 side chains all reside more than 8.2 Å from either active-site histidine residue [PDB entry 1rph (*36*)]. Yet, the binding of 3′−UMP to the active site is weakened significantly upon replacement of the distal residues with alanine (Table 4), even though the active-site histidine residues are more likely to be protonated (Table 3). What is the physical basis for this counterintuitive effect?

The free energy of the protein·nucleotide complex is relatively immutable. Eftink and Biltonen (*16*) examined the hydrolysis of cytidine cyclic 2′,3′-phosphate by RNase A in detail. They concluded that when a substrate is bound to the active site, it is relatively impervious to the ionic strength or dielectric constant of the surrounding solution. In the RNase A·3′−UMP complex, the cationic P0 and P2 subsites can interact via long-range Coulombic interactions with both the cationic histidine residues and the anionic nucleotide. These repulsive forces and attractive forces should be of nearly equal but opposite magnitude, negating a net contribution from the distal subsites.

Enzymatic catalysis was once described as resulting from the destabilization of the unliganded enzyme (*93*, *94*) rather than the stabilization of the transition state that occurs along the reaction coordinate. In both of these scenarios, enzymes lower the activation barrier of the reaction, but by different means. In the former scenario, enzymic active sites are viewed as tense or entatic—poised for catalysis even in the absence of substrate. More entatic enzymes are better catalysts. Although the latter description of enzymatic catalysis is now accepted more widely, the former description provides a conceptual framework with which to describe our binding data.

The entasis of an unliganded ribonuclease corresponds to its nucleotide affinity. Wild-type RNase A in a low-salt solution has a highly cationic active-site cleft. Accordingly, the pK_a values of His12 and His119 are low (Table 3), as is the $\Delta G°$ value for binding 3′−UMP (Table 4). By comparison, K7A/R10A/K66A RNase A in a high-salt solution has a much less cationic active-site cleft. The pK_a and $\Delta G°$ values are high (Tables 3 and 4). Wild-type RNase A at high salt and K7A/R10A/K66A RNase A at low salt have intermediate entasis. Thus, the binding of ligand is most favored when it relieves the most tension.

A detailed description of RNase A·3′−CMP complex formation by Biltonen and co-workers has yielded much information about the thermodynamic basis for the binding of nucleotides to RNase A (*86*−*88*). Their work and ours are consistent with the following picture. The enthalpic component of the binding free energy is derived primarily from favorable van der Waals interactions and hydrogen bonds between the base of the bound nucleotide and the B1 subsite of RNase A and from the protonation of His12 and His119. Although the protonation of histidine residues is favored enthalpically [$\Delta H°_{protonation} = -6.3$ kcal/mol (*95*)], it is disfavored entropically. The entropic component to the binding free energy is a summation of favorable and unfavorable terms. Attractive Coulombic interactions between the protonated histidine residues and the bound nucleotide are entropically favorable because of the release of bound ions or water molecules. Yet, restricting the translation and rotation of the nucleotide upon binding is entropically unfavorable.

Conclusions. ^{1}H NMR spectroscopy and isothermal titration calorimetry coupled with X-ray diffraction analyses of K7A/R10A/K66A RNase A and the K7A/R10A/K66A RNase A·3′−UMP complex has enabled us to reveal the effect of the Lys7, Arg10, and Lys66 side chains on the active-site of RNase A. The increased pK_a values of His12 and His119 upon replacing Lys7, Arg10, and Lys66 with alanine residues and the subsequent effects on the kinetics of UpA cleavage and the thermodynamics of 3′−UMP binding indicate that Lys7, Arg10, and Lys66 affect the enzymic active site through long-range Coulombic interactions. We suspect that such long-range Coulombic interactions are a common feature of enzymatic catalysis.

ACKNOWLEDGMENT

We thank Drs. David J. Quirk and John L. Markley and the staff of the NMRFAM for assistance with NMR experiments and data analysis, Dr. Darrell R. McCaslin for assistance in collecting calorimetry data, and Drs. Ivan Rayment and Hazel M. Holden and the members of their research groups for the use of their X-ray data collection and computational facilities, which are supported by Grant BIR-9317398 (NSF). We also thank Dr. Adam H. Fisher, Bradley R. Kelemen, June M. Messmore, Chiwook Park, Kimberly M. Taylor, Jon F. Wilkins, and Kenneth J. Woycechowsky for helpful discussions and comments on the manuscript.

REFERENCES

1. Gutfreund, H., and Knowles, J. R. (1967) *Essays Biochem. 3*, 25−72.

2. Jencks, W. P. (1969) *Catalysis in Chemistry and Enzymology*, McGraw-Hill, New York.
3. Sharp, K., Fine, R., and Honig, B. (1987) *Science 236*, 1460−1463.
4. Jackson, S. E., and Fersht, A. R. (1993) *Biochemistry 32*, 13909−13916.
5. Russell, A. J., Thomas, P. G., and Fersht, A. R. (1987) *J. Mol. Biol. 193*, 803−813.
6. Kokesh, F. C., and Westheimer, F. H. (1971) *J. Am. Chem. Soc. 93*, 7270−7274.
7. Frey, P. A., Kokesh, F. C., and Westheimer, F. H. (1971) *J. Am. Chem. Soc. 93*, 7266−7269.
8. Schmidt, D. E., and Westheimer, F. H. (1971) *J. Am. Chem. Soc. 10*, 1249−1253.
9. Highbarger, L. A., Gerlt, J. A., and Kenyon, G. L. (1996) *Biochemistry 35*, 41−46.
10. Raines, R. T. (1998) *Chem. Rev. 98*, 1045−1066.
11. Findlay, D., Herries, D. G., Mathias, A. P., Rabin, B. R., and Ross, C. A. (1961) *Nature 190*, 781−784.
12. Thompson, J. E., and Raines, R. T. (1994) *J. Am. Chem. Soc. 116*, 5467−5468.
13. Cuchillo, C. M., Parés, X., Guasch, A., Barman, T., Travers, F., and Nogués, M. V. (1993) *FEBS Lett. 333*, 207−210.
14. Thompson, J. E., Venegas, F. D., and Raines, R. T. (1994) *Biochemistry 33*, 7408−7414.
15. del Rosario, E. J., and Hammes, G. G. (1969) *Biochemistry 8*, 1884−1889.
16. Eftink, M. R., and Biltonen, R. L. (1983) *Biochemistry 22*, 5123−5134.
17. Kartha, G., Bello, J., and Harker, D. (1967) *Nature 213*, 862−865.
18. Crestfield, A. M., Stein, W. H., and Moore, S. (1962) *Arch. Biochem. Biophys., Suppl. 1*, 217−222.
19. Pincus, M., Thi, L. L., and Carty, R. P. (1975) *Biochemistry 14*, 3653−3661.
20. Lennette, E. P., and Plapp, B. V. (1979) *Biochemistry 18*, 3938−3946.
21. Meadows, D. H., Roberts, G. C. K., and Jardetzky, O. (1969) *J. Mol. Biol. 45*, 491−511.
22. Rüterjans, H., and Witzel, H. (1969) *Eur. J. Biochem. 9*, 118−127.
23. Cohen, J. S., Griffen, J. H., and Schechter, A. N. (1973) *J. Biol. Chem. 248*, 4305−4310.
24. Haar, W., Maurer, W., and Rüterjans, H. (1974) *Eur. J. Biochem. 44*, 201−211.
25. Markley, J. L. (1975) *Biochemistry 14*, 3546−3553.
26. Markley, J. L. (1975) *Acc. Chem. Res. 8*, 70−80.
27. Markley, J. L. (1975) *Biochemistry 14*, 3554−3561.
28. Markley, J. L., and Finkenstadt, W. R. (1975) *Biochemistry 14*, 3562−3566.
29. Fisher, B. M., Ha, J.-H., and Raines, R. T. (1998) *Biochemistry 37*, 12121−12132.
30. Ogilvie, K. K., Beaucage, S. L., Schifman, A. L., Theriault, N. Y., and Sadana, K. L. (1978) *Can. J. Chem. 56*, 2768−2780.
31. Beaucage, S. L., and Caruthers, M. H. (1981) *Tetrahedron Lett. 22*, 1859−1862.
32. Sela, M., Anfinsen, C. B., and Harrington, W. F. (1957) *Biochim. Biophys. Acta 26*, 502−512.
33. Beaven, G. H., Holiday, E. R., and Johnson, E. A. (1955) in *The Nucleic Acids, Chemistry and Biology* (Chargraff, E., and Davidson, J. N., Ed.) pp 493−553, Academic Press, New York.
34. Scopes, R. K. (1994) *Protein Purification: Principles and Practice*, Springer-Verlag, New York.
35. Ferrin, T. E., Huang, C. C., Jarvis, L. E., and Langridge, R. (1988) *J. Mol. Graphics 6*, 13−27.
36. Zegers, I., Maes, D., Dao-Thi, M., Poortmans, F., Palmer, R., and Wyns, L. (1994) *Protein Sci. 3*, 2322−2339.
37. Nicholls, A., Sharp, K. A., and Honig, B. (1991) *Proteins: Struct., Funct., Genet. 11*, 281−296.
38. Righetti, P. G., Gianazza, E., Gelfi, C., and Chiari, M. (1990) in *Gel Electrophoresis of Proteins: A Practical Approach* (Hames, B. D., and Rickwood, D., Ed.) pp 149−216, Oxford University Press, Oxford.
39. Righetti, P. G. (1983) in *Laboratory Techniques in Biochemistry and Molecular Biology* (Work, T. S., and Burdon, R. H., Ed.) Vol. 11, pp 148−267, Elsezier Science, Amsterdam.
40. Ui, N. (1971) *Biochim. Biophys. Acta 229*, 567−581.
41. Kabsch, W. (1988) *J. Appl. Crystallogr. 21*, 916−924.
42. Kabsch, W. (1988) *J. Appl. Crystallogr. 21*, 67−71.
43. Schultz, L. W., Quirk, D. J., and Raines, R. T. (1998) *Biochemistry 37*, 8886−8898.
44. Tronrud, D. E., Ten-Eyck, L. F., and Matthews, B. W. (1987) *Acta Crystallogr., Sect. A 43*, 489−501.
45. Jones, T. A. (1985) *Methods Enzymol. 115*, 157−171.
46. Thompson, J. E. (1995) Ph.D. Thesis, University of Wisconsin−Madison.
47. Cleland, W. W. (1979) *Methods Enzymol. 63*, 103−138.
48. Shrager, R. I., Cohen, J. S., Heller, S. R., Sachs, D. H., and Schechter, A. N. (1972) *Biochemistry 11*, 541−547.
49. Chivers, P. T., Prehoda, K. E., Volkman, B. F., Kim, B.-M., Markley, J. L., and Raines, R. T. (1997) *Biochemistry 36*, 14985−14991.
50. Karpeisky, M. Y., and Yakovlev, G. I. (1981) *Sov. Sci. Rev., Sect. D 2*, 145−257.
51. Quirk, D. J. (1996) Ph.D. Thesis, University of Wisconsin−Madison.
52. Nogués, M. V., Vilanova, M., and Cuchillo, C. M. (1995) *Biochim. Biophys. Acta 1253*, 16−24.
53. Boix, E., Nogués, M. V., Schein, C. H., Benner, S. A., and Cuchillo, C. M. (1994) *J. Biol. Chem. 269*, 2529−2534.
54. Brünger, A. T., Brooks, C. L., III, and Karplus, M. (1985) *Proc. Natl. Acad. Sci. U.S.A. 82*, 8458−8462.
55. Gilliland, G. L. (1997) in *Ribonucleases: Structures and Functions* (D'Alessio, G., and Riordan, J. F., Ed.) pp 306−341, Academic Press, New York.
56. González, C., Santoro, J., and Rico, M. (1997) in *Ribonucleases: Structures and Functions* (D'Alessio, G., and Riordan, J. F., Ed.) pp 343−381, Academic Press, New York.
57. Schultz, L. W., Hargraves, S. R., Klink, T. A., and Raines, R. T. (1998) *Protein Sci. 7*, 1620−1625.
58. Borkakoti, N., Moss, D. A., and Palmer, R. A. (1982) *Acta Crystallogr., Sect. B 38*, 2210−2217.
59. Borkakoti, N. (1983) *Eur. J. Biochem. 132*, 89−94.
60. Fedorov, A. A., Joseph-McCarthy, D., Fedorov, E., Sirakova, D., Graf, I., and Almo, S. C. (1996) *Biochemistry 35*, 15962−15979.
61. Jenkins, H. D. B., and Thakur, K. P. (1979) *J. Chem. Educ. 56*, 576−577.
62. Richards, F. M., and Vithayathil, P. J. (1959) *J. Biol. Chem. 234*, 1459−1465.
63. Hofmann, K., Finn, F. M., Limetti, M., Montibeller, J., and Zanetti, G. (1966) *J. Am. Chem. Soc. 88*, 3633−3636.
64. Osterhout, J. J., Jr., Baldwin, R. L., York, E. J., Stewart, J. M., Dyson, H. J., and Wright, P. E. (1989) *Biochemistry 28*, 7059−7064.
65. Finkelstein, A. V., Badretdinov, A. Y., and Ptitsyn, O. B. (1991) *Proteins: Struct., Funct., Genet. 10*, 287−299.
66. Kato, I., and Anfinsen, C. B. (1969) *J. Biol. Chem. 244*, 1004−1007.
67. Labhardt, A. M., and Baldwin, R. L. (1979) *J. Mol. Biol. 135*, 231−244.
68. Brems, D. N., and Baldwin, R. L. (1984) *J. Mol. Biol. 80*, 1141−1156.
69. Gross, E., and Witkop, B. (1962) *J. Biol. Chem. 237*, 1856−1860.
70. Rico, M., Gallego, E., Santoro, J., Bermejo, F. J., Nieto, J. L., and Herranz, J. (1984) *Biochem. Biophys. Res. Commun. 123*, 757−763.
71. Fairman, R., Shoemaker, K. R., York, E. J., Stewart, J. M., and Baldwin, R. L. (1990) *Biophys. Chem. 37*, 107−119.
72. Shoemaker, K. R., Kim, P. S., Brems, D. N., Marqusee, S., York, E. J., Chaiken, I. M., Stewart, J. M., and Baldwin, R. L. (1985) *Proc. Natl. Acad. Sci. U.S.A. 82*, 2349−2353.
73. Kraulis, P. J. (1991) *J. Appl. Crystallogr. 24*, 916−924.

74. delCardayré, S. B., and Raines, R. T. (1995) *J. Mol. Biol. 252*, 328−336.
75. Wlodawer, A., Miller, M., and Sjölin, L. (1983) *Proc. Natl. Acad. Sci. U.S.A. 80*, 3628−3631.
76. Antosiewicz, J., McCammon, J. A., and Gilson, M. K. (1996) *Biochemistry 35*, 7819−7833.
77. Russell, A. J., and Fersht, A. R. (1987) *Nature 328*, 496−500.
78. delCardayré, S. B., Ribó, M., Yokel, E. M., Quirk, D. J., Rutter, W. J., and Raines, R. T. (1995) *Protein Eng. 8*, 261−273.
79. Wyman, J., and Gill, S. J. (1990) *Binding and Linkage: Functional Chemistry of Biological Macromolecules*, University Science Books, Mill Valley, CA.
80. Kirkwood, J. G., and Westheimer, F. H. (1938) *J. Chem. Phys. 6*, 506−512.
81. Edsall, J. T., Martin, R. B., and Hollingworth, B. R. (1958) *Proc. Natl. Acad. Sci. U.S.A. 44*, 505−518.
82. Messmore, J. M., Fuchs, D. N., and Raines, R. T. (1995) *J. Am. Chem. Soc. 117*, 8057−8060.
83. Richards, F. M., and Wyckoff, H. W. (1971) *The Enzymes IV*, 647−806.
84. Irie, M., Mikami, F., Monma, K., Ohgi, K., Watanabe, H., Yamaguchi, R., and Nagase, H. (1984) *J. Biochem. 96*, 89−96.
85. Bolen, D. W., Flögel, M., and Biltonen, R. (1971) *Biochemistry 10*, 4136−4140.
86. Flogel, M., Albert, A., and Biltonen, R. L. (1975) *Biochemistry 14*, 2616−2621.
87. Flogel, M., and Biltonen, R. L. (1975) *Biochemistry 14*, 2603−2609.
88. Flogel, M., and Biltonen, R. L. (1975) *Biochemistry 14*, 2610−2615.
89. Wiseman, T., Williston, S., Brandts, J. F., and Nan, L.-N. (1989) *Anal. Biochem. 179*, 131−137.
90. Eftink, M. R., Anusiem, A. C., and Biltonen, R. L. (1983) *Biochemistry 22*, 3884−3896.
91. Mauk, M. R., Barker, P. D., and Mauk, A. G. (1991) *Biochemistry 30*, 9873−9881.
92. Raman, C. S., Allen, M. J., and Nall, B. T. (1995) *Biochemistry 34*, 5831−5838.
93. Vallee, B. L., and Williams, R. J. P. (1968) *Proc. Natl. Acad. Sci. U.S.A. 59*, 498−505.
94. Williams, R. J. P. (1971) *Cold Spring Harbor Symp. Quantum Biol. 36*, 53−62.
95. Shiao, D. D. F., and Sturtevant, J. M. (1976) *Biopolymers 15*, 1201−1211.

BI981369S